CMS Physics Analysis Summary

Contact: cms-pag-conveners-exotica@cern.ch 2012/07/06

Search for multi-charged Heavy Stable Charged Particles at $\sqrt{s} = 7$ TeV

The CMS Collaboration

Abstract

Many models of new physics allow for particles that are massive, long-lived, and have an electric charge greater than that of the electron, e. We perform a search for evidence of such particles using 5.0 fb^{-1} of data collected with the CMS detector. The distinctive detector signatures of such particles are that they are slow-moving and highly ionizing. By using the silicon tracker for ionization measurements and the muon system for time of flight, we are sensitive to particles with charge of one to five times the electron charge. We find no significant excess compared to the standard model expectation and set limits on the pair production cross section using a fourth generation model. We exclude masses below 427, 489, 545, 572 and 504 GeV/c^2 for charges of 1e, 2e, 3e, 4e and 5e, respectively. Limits on the electric charge for masses of 100, 200, 300, 400, 450, and 500 GeV/c^2 are also obtained, excluding charges 1–5e, 1–5e, 1–5e, 1–5e, 1.3–5e, and 2.2–5e, respectively.

1 Introduction

Heavy stable charged particles (HSCPs) are massive (>100 GeV/c^2), long-lived ($c\tau \gtrsim 1$m), and electrically charged particles that are predicted by many beyond the standard model (BSM) theories [1, 2]. Previous searches at colliders [3–9] have generally used the distinctive signatures of long time-of-flight (TOF), large ionization per path length ($\mathrm{d}E/\mathrm{d}x$), or delayed decay. Recent reviews of experimental searches for HSCPs are available in Refs. [1, 10, 11].

While most searches have assumed the HSCP electric charge, Q, to be $\pm 1e$, they can be fractionally, singly, or multiply charged. An example of a fractionally charged massive particle is a heavy free quark (or squark). Singly charged massive particles include long-lived staus ($\widetilde{\tau}$) from gauge-mediated SUSY breaking (GMSB) [12] or stops ($\widetilde{\mathrm{t}}$) bound with standard model (SM) quarks (R-hadrons) [2, 13–15]. Examples of multi-charged HSCPs are Q-balls [16], stable micro black-hole remnants [17], dyons [18], and doubly charged leptons [19]. The doubly charged HSCPs can be bounded into "neutral" stable atoms forming cold dark matter, as described in the Almost Commutative (AC) geometrical framework [19].

This analysis focuses on a search for multi-charged HSCPs with a Q of $1e$–$5e$ and with mass >100 GeV/c^2 using data collected with the Compact Muon Solenoid (CMS) detector during the 2011 proton-proton run of the Large Hadron Collider (LHC) at CERN. Multi-charged HSCPs are identified using their large $\mathrm{d}E/\mathrm{d}x$ and long TOF. The ATLAS collaboration has previously searched for highly ionizing particles with a Q of $6e$–$17e$ [8].

2 CMS Detector

The central feature of the CMS apparatus is a superconducting solenoid of 6 m internal diameter. Within the field volume are the silicon pixel and strip tracker, the crystal electromagnetic calorimeter (ECAL), and the brass/scintillator hadron calorimeter (HCAL). Muons are measured in gas-ionization detectors embedded in the steel return yoke. In addition to the barrel and endcap detectors, CMS has extensive forward calorimetry. CMS uses a right-handed coordinate system, with the origin at the nominal interaction point, the x-axis pointing to the center of the LHC ring, the y-axis pointing up (perpendicular to the LHC plane), and the z-axis along the counterclockwise-beam direction. The polar angle, θ, is measured from the positive z-axis and the azimuthal angle, ϕ, is measured in the x-y plane. The muons are measured in the pseudorapidity ($\eta \equiv -\ln\tan(\theta/2)$) range $|\eta| < 2.4$, with detection planes made using three technologies: drift tubes (DT), cathode strip chambers (CSC), and resistive plate chambers (RPC). DT and CSC detectors are installed in the barrel at $|\eta| < 1.2$ and in the endcaps at $0.9 < |\eta| < 2.4$ respectively whereas RPCs cover the range $|\eta| < 1.6$. The inner tracker measures charged particles within the pseudorapidity range $|\eta| < 2.5$. It provides an impact parameter resolution of ~ 15 μm and a p_T resolution of ~ 1.5 % for charged particles with a p_T of 100 GeV/c, where p_T is the component of the momentum in the x-y plane. The CMS trigger consists of a two-stage system. The first level (Level-1) of the CMS trigger system, composed of custom hardware processors, uses information from the calorimeters and muon detectors to select a subset of the events. The High Level Trigger (HLT) processor farm further decreases the event rate from around 100 kHz to around 300 Hz, before data storage. A detailed description of the CMS detector can be found elsewhere [20].

3 Monte Carlo Simulation

To simulate our signal, we use a long-lived fourth generation lepton (τ') model from PYTHIA v6.422 [21] in which a pair of leptons ($\tau'\bar{\tau}'$) are produced through the Drell-Yan (DY) process with neutral current, $Z^\star/\gamma^\star$. The τ' is set to be stable. Samples are generated for masses 100–600 GeV/c^2 and Q= $1e$−$5e$. Figure 1 shows the p_T, η and β distributions for a τ' with $Q = 1e$ and masses of 100, 400 and 1000 GeV/c^2, where β is the speed of the τ' relative to the speed of light in vacuum.

As the mass of the τ' increases, the p_T distribution becomes harder, the β distribution becomes more non-relativistic and the τ' tends to be centrally produced. The kinematics of a multi-charged HSCP (τ') do not change much as a function of Q. The SM background processes used for this analysis consist of Drell-Yan, QCD, $W^\pm$, $t\bar{t}$ and diboson processes. These samples are made using various generators such as PYTHIA, MADGRAPH [22] and TAUOLA [23]. . We use the CTEQ6L1 [24] parton distribution function (PDF) set with D6T tune [25, 26].

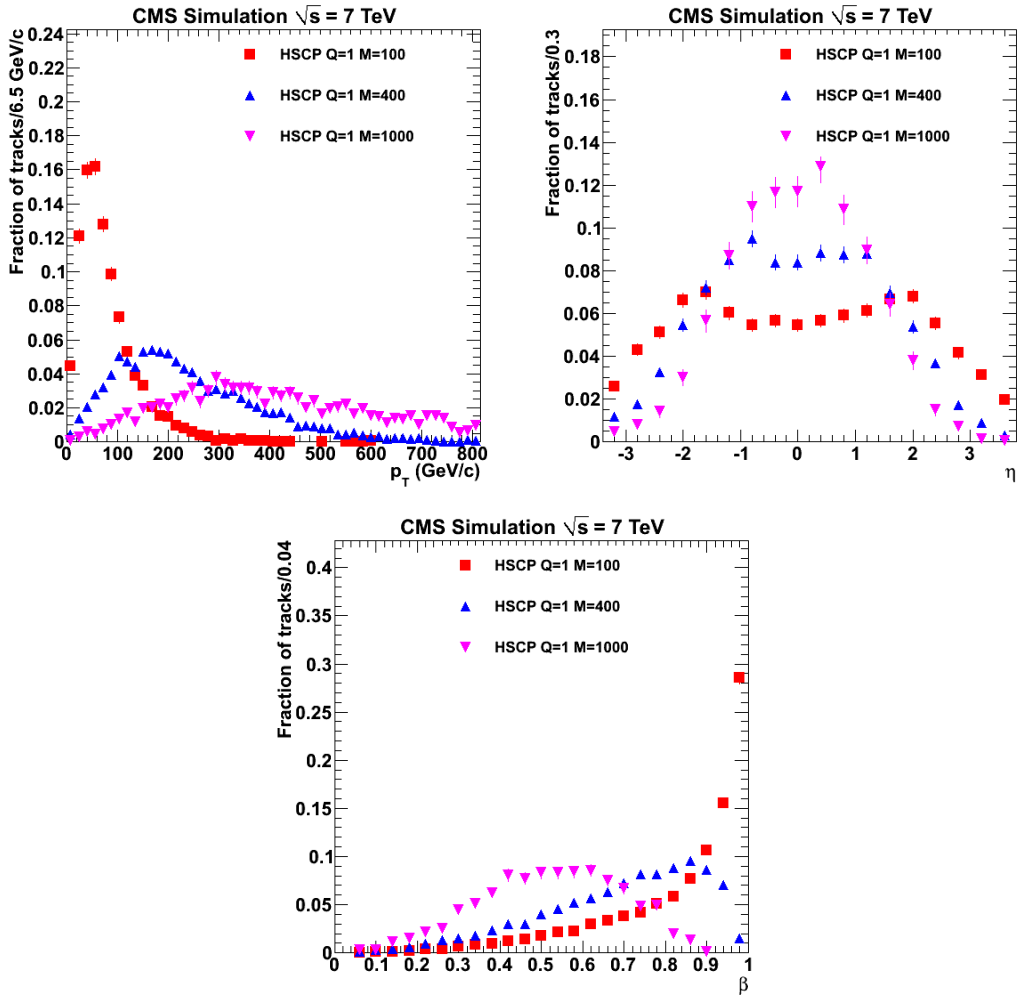

Figure 1: Distributions of p_T, η and β for a long-lived fourth generation singly charged HSCP (τ') with masses 100, 400, and 1000 GeV/c^2.

Simulated events are passed through GEANT4 v9.2 [27, 28] to model the detector. Interactions of the multi-charged HSCP with appropriate Q have been added. Monte Carlo (MC) events are overlaid with simulated minimum bias events to reproduce the expected distribution of the

number of inelastic collisions per bunch crossing (pile-up) observed in data.

In this analysis, $\mathrm{d}E/\mathrm{d}x$ is calculated using the silicon tracker by combining energy measurements in both the pixel and strip detectors. Individual channels are combined with neighboring channels above a threshold to form clusters. All clusters are used to reconstruct tracks. We apply a cleaning procedure to clusters in the silicon strip detector associated with candidate tracks and we remove clusters that are inconsistent with a single particle profile. The cleaning procedure is designed to reduce contamination from overlapping tracks, nuclear interactions and hard-δ rays. For each candidate track, two variables are calculated using the remaining clusters, I_h and I_{as}:

$$I_h = \left(\frac{1}{N}\sum_i c_i^k\right)^{1/k}, \tag{1}$$

where c_i is the charge per unit path length in the sensitive part of the silicon detector of the i-th track measurement and $k = -2$; and

$$I_{as} = \frac{3}{N} \times \left(\frac{1}{12N} + \sum_{i=1}^{N}\left[P_i \times \left(P_i - \frac{2i-1}{2N}\right)^2\right]\right), \tag{2}$$

where N is the number of measurements in the silicon-strip detectors, P_i is the probability for a minimum–ionizing particle (MIP) to produce a charge smaller or equal to that of the i–th measurement for the observed path length in the detector, and the sum is over the track measurements ordered in terms of increasing P_i. The I_h estimator is computed using both silicon strip and pixel measurements while the I_{as} estimator is computed using only silicon strip measurements.

The $\mathrm{d}E/\mathrm{d}x$ for HSCPs is roughly proportional to $\frac{Q^2}{\beta^2}$ [29] for the range $0.1 < \beta < 0.9$. Therefore, a lower β will give rise to higher than normal ionization energy loss for a HSCP and a larger Q will greatly increase the ionization. A MIP has an I_h value of approximately 3 MeV/cm and I_{as} value near zero. Multi-charged HSCPs tend to have much larger I_h and I_{as} due to their lower β and higher Q^2. Each individual silicon channel has a dynamic range of $\sim$0–3 times that of a MIP. Larger energy depositions are recorded as a saturation and included in the $\mathrm{d}E/\mathrm{d}x$ calculations as $\sim$3 MIPs.

TOF is measured using timing from the muon system. For muons produced at the primary vertex, the TOF delay, δ_t, is expected to be consistent with zero within the time measurement accuracy. Prompt HSCP candidates would be largely non-relativistic, resulting in a δ_t value greater than zero. A single δ_t measurement can be used to determine the track $1/\beta$ via the equation:

$$\frac{1}{\beta} = 1 + \frac{c\delta_t}{L} \tag{3}$$

where L is the flight distance and c is the speed of light. The final track $1/\beta$ value is calculated as the weighted average of the $1/\beta$ measurements associated with the track. The resolution of $1/\beta$ is 0.06 in the regions occupied by both the DTs and CSCs. Additional details of the $\mathrm{d}E/\mathrm{d}x$ and $1/\beta$ measurements may be found in Ref. [9].

4 Trigger and Data Selection

The long lifetime of the multi-charged HSCPs will allow them to travel to the outermost parts of the CMS detector. Hence, we can identify them using the muon system. Events must pass

a trigger that requires a muon with $p_{\mathrm{T}} > 40$ GeV/c and $|\eta| < 2.1$. The first level of the muon trigger accepts signals in the RPC detectors that occur within the 25 ns time window centered on the collision bunch crossing or within the following 25 ns when there are no collisions. The CSC and DT detectors only use the in-time 25 ns window. The extended window allows for increased acceptance for slow moving particles that arrive late to the muon system.

The trigger and offline reconstruction assume that all tracks have charge $\pm 1e$. Due to the scaling of their reconstructed p_T by a factor of their Q and the Q^2 enhancement in their energy loss, the trigger efficiency of multi-charged HSCPs decreases as their Q increases. The p_T distribution of multi-charged HSCPs becomes harder as their mass increases, yielding an increase in their trigger efficiency for larger masses. The efficiency for the muon trigger and the offline selections mentioned in the next paragraph, is $\sim 10^{-3}$ for a multi-charged HSCP with $Q = 6e$. Hence, we limit our search to multi-charged HSCPs with $Q = 1e$–$5e$.

For offline pre-selection, candidates were required to have p_{T} (as measured by the inner tracker) greater than 45 GeV/c, the relative uncertainty on the p_T smaller than 0.25, track $\chi^2/d.o.f. < 5$, $|\eta| < 2.1$, and impact parameter $\sqrt{d_z^2 + d_{xy}^2} < 0.5$ cm where d_z and d_{xy} are the longitudinal and transverse impact parameters with respect to the reconstructed primary vertex that minimizes d_Z. Candidates were required to have at least two measurements in the silicon pixel detectors and at least eleven measurements in the inner tracking detectors before cleaning. No more than 20% of the inner tracker layers were allowed to be missing between the first and last measurement of the track. Candidates were required to have at least six silicon strip measurements passing the cleaning criteria and, therefore, used for the dE/dx measurement. Candidate tracks were required to have $I_h > 3$ MeV/cm for the initial selection. The number of independent measurements used for the TOF computation was required to be greater than seven. For β measured from TOF, $1/\beta$ must be greater than 1 and $\sigma_{1/\beta} < 0.07$. Tracker isolation in the form of $\sum p_T/p_T < 0.10$ was used where $\sum p_T$ is the sum of the p_T of all tracks, excluding the candidate track, within a cone of radius $\Delta R = \sqrt{\Delta\phi^2 + \Delta\eta^2} = 0.3$ along the candidate track direction. This isolation selection is used to veto on jets which can fake our signal characteristics of large values of I_{as} and $1/\beta$.

Since the reconstructed p_{T} of multi-charged HSCPs is scaled by a factor of their charge, we maximize our signal acceptance by keeping the p_{T} threshold low for the pre-selection. Also, p_{T} is not used as a discriminating variable in the final selection.

5 Background Estimate and Search

SM particles will generally deposit MIP energies in the tracker (low values of I_{as}) and have TOF consistent with the speed of light ($1/\beta \approx 1$). Multi-charged HSCPs, on the other hand, should deposit larger energies in the silicon (higher values of I_{as}) and have longer TOF ($1/\beta > 1$). Figure 2 show the distributions of these variables for data and various signals after candidate selection. We use these variables to select a signal region with a good signal-to-background ratio. We also use a data-driven technique to estimate the contributions from SM particles to this region.

The candidates passing the pre-selection described above were used for both the background estimate and the search. The final signal candidates are defined as those with I_{as} and $1/\beta$ greater than threshold values optimized for each model and mass point. Figure 3 shows the $1/\beta$ spectrum for different I_{as} regions in data. We observe that the $1/\beta$ spectra in each of the I_{as} regions have the same shape, showing no evidence of correlations. A method, termed as the ABCD method, exploiting this non-correlation between I_{as} and $1/\beta$ measurements for SM

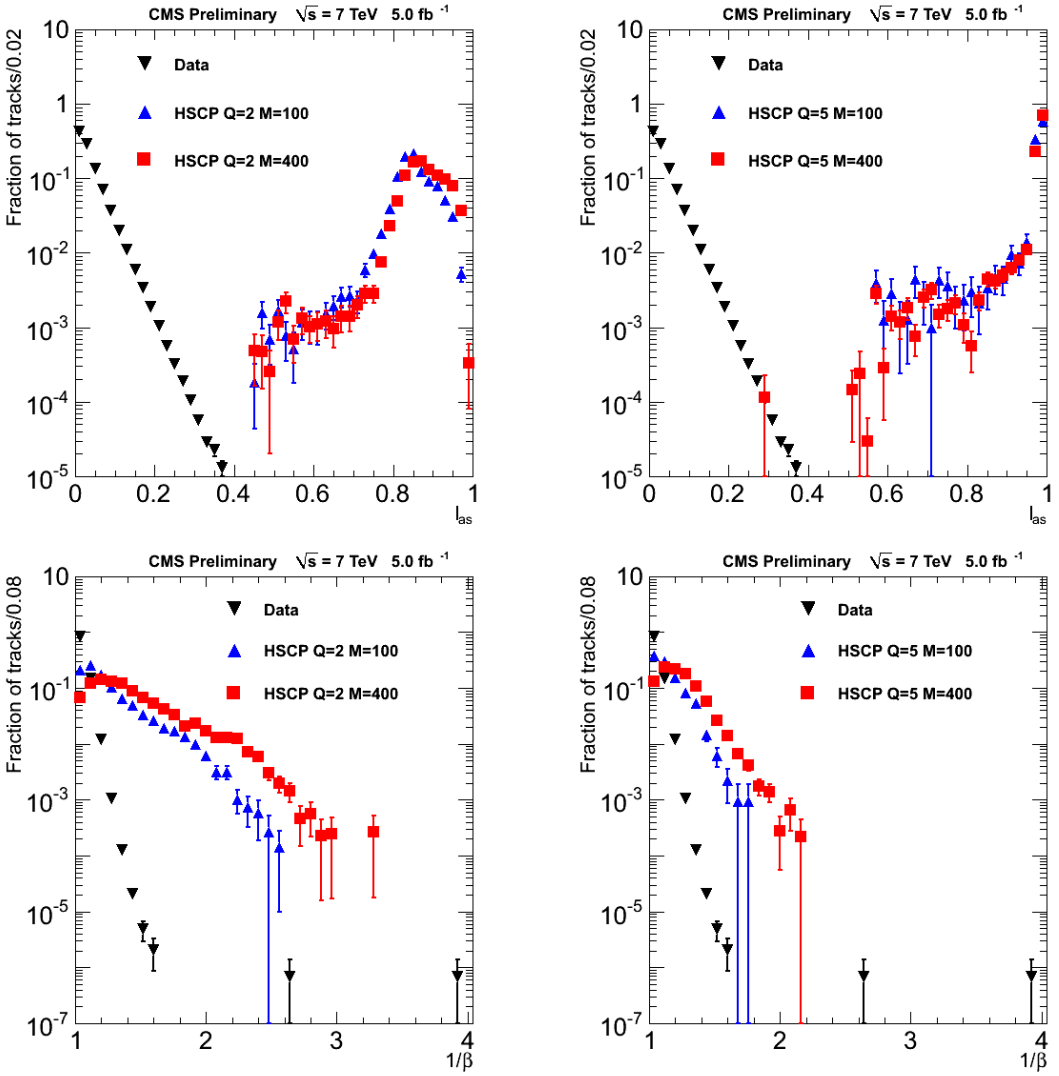

Figure 2: Distributions of I_{as} (top row) and $1/\beta$ (bottom row) for data (black inverted triangles) and multi-charged HSCP signal with mass 100 GeV/c^2 (blue triangles) and 400 GeV/c^2 (red squares). The left column shows signal with $Q = 2e$ while the right column shows $Q = 5e$.

particles, was used to estimate their contribution within the signal sample. The number of SM particles expected to pass both the final I_{as} and $1/\beta$ thresholds was estimated as $D = BC/A$, where A is the number of candidates that fail both the I_{as} and $1/\beta$ selections and B (C) is the number of candidates that pass only the $1/\beta$ (I_{as}) selection. The final analysis compares the predicted number of expected events in the signal region (D) with the observed number.

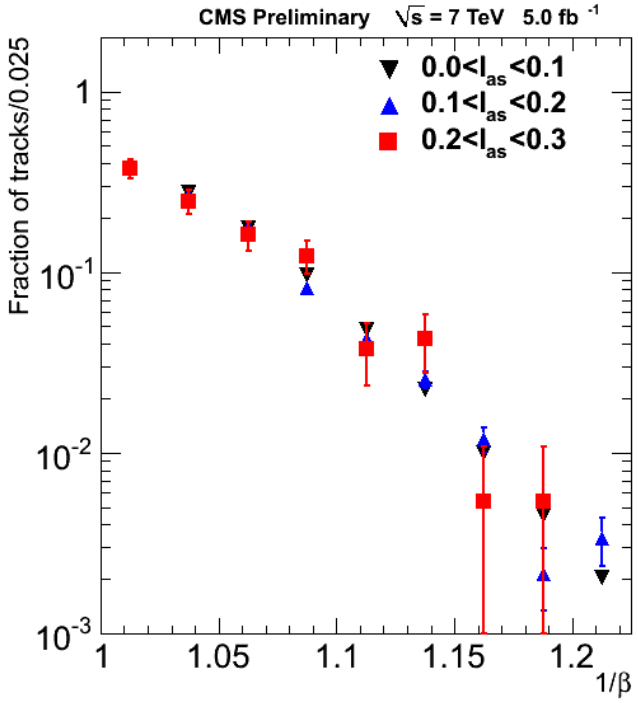

Figure 3: Distributions of $1/\beta$ for different I_{as} regions in data.

We check the performance of the ABCD method with these variables using a sample with loose I_{as} and $1/\beta$ thresholds of 0.05 and 1.075, respectively. The number of predicted events in the D region is 57754$\pm$ 179 for this loose sample. The number of observed events is 6% fewer. Figure 4 compares the I_{as} spectrum in the D region with that of the C region scaled by B/A.

6 Systematic Uncertainties

In addition to the statistical uncertainty on D, we estimate a systematic uncertainty on the background estimation method. For the candidate pre-selection, we require $1/\beta > 1.0$. We define an alternate data sample consisting of events with $1/\beta < 1.0$. This phase space encompasses E and F regions, where events in the E (F) region fail (pass) the the I_{as} selection. We use the E, F, and B regions to predict the number of tracks in the D region ($D' = BF/E$). We compare the two predictions (D and D') for all possible final values of the I_{as} and $1/\beta$ selections. Figure 5 is a representative plot showing D and D' for $1/\beta$ selection of 1.20 and all possible I_{as} selections. The ratio of the two predicted number of tracks (D/D') is also shown. We observe good agreement between the two predictions for low values of I_{as} cuts. For the maximum allowed threshold I_{as} = 0.40, the predictions agree within 20%. Therefore, we quantify the background uncertainty as 20%.

The signal acceptance is estimated using simulation and several uncertainties are applicable. We evaluate the systematic contribution due to differences in the I_{as} and $1/\beta$ scales in data and

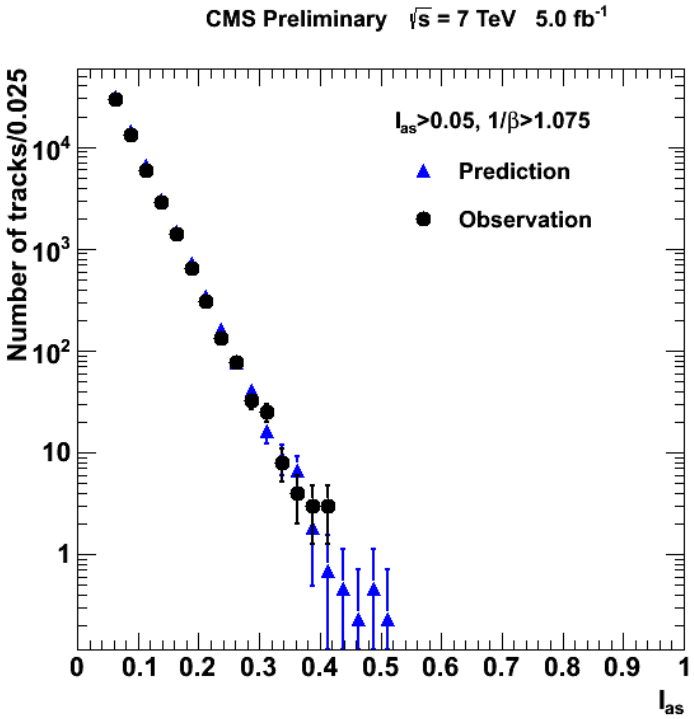

Figure 4: Distribution of I_{as} for the loose sample for the D region (black circles) and the C region scaled by the ABCD method (blue triangles).

simulation. The systematic uncertainty in the pile-up matching procedure is also estimated.

The I_{as} scale uncertainty was evaluated by studying low-energy proton data which found the I_{as} scale has a resolution of 0.083 and a shift of 0.015. We study this by shifting the I_{as} value by adding two terms: (a) a random number from a Gaussian with a *mean* of 0.00 and a *width* of 0.083, and (b) a constant of 0.015. The systematic uncertainty due to the I_{as} scale uncertainty is quantified as the incremental change in the signal efficiency for the final selection due to the I_{as} shift. For all signal points, the systematic contribution is less than 1%.

The $1/\beta$ scale uncertainty is evaluated by shifting its value by -0.02(-0.003) for the CSC(DT) region (difference between data and SM background MC), and the incremental change in the signal efficiency for the final selection is taken as the systematic uncertainty due to $1/\beta$ scale. For most signal points, the $1/\beta$ systematic is less than 5%. The uncertainty increases for higher Q and lower masses, where the events in the final selection are much farther from the core of the distributions. We also compute the statistical uncertainty on the final selection to properly absorb the effect of the final selection lying in the tail regions of the $1/\beta$ distributions.

The uncertainty on the pile-up matching procedure was studied by shifting the number of pile-up vertices in our signal MC by 0.6. The resulting change in signal efficiency for the final selection is quantified as the uncertainty due to the discrepancy in the distribution of the number of pile-up collisions in data and simulation. The change in signal efficiency for all the signal points is less than 1%.

The muon trigger efficiency differs by up to 5% between data and simulation for all energies [30]. We consider two additional uncertainties on the muon trigger due to imperfect simulation of the synchronization of muon trigger electronics and the variation in the total CMS detector material in front of the muon system. The former is studied by shifting the timing of

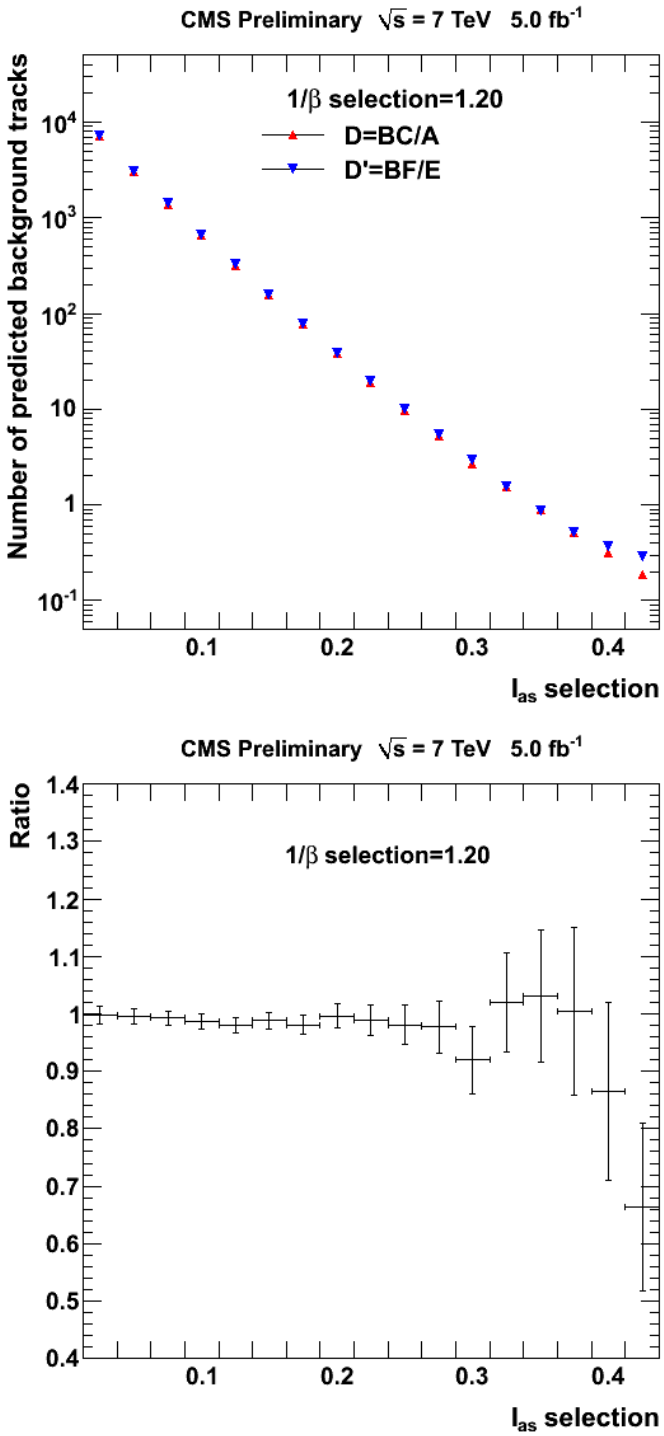

Figure 5: The estimated number of background tracks in the signal region for the D (red) and D′ (blue) methods for a fixed $1/\beta$ threshold of 1.20. The bottom plot shows the ratio D/D′.

simulated hits and redoing the HLT emulation on the new sample [31]. The effect is found to be less than 9%. The material budget used in the simulation is varied by increasing the HCAL material density by a conservative 5%, as determined from the single particle validation study of GEANT4 simulation [32]. With this change, the muon trigger efficiency decreases by less than 20% for low mass and large Q which show the largest deviation. Therefore, we conservatively quantify the systematics due to the uncertainty in the material budget in the simulation as 20%.

The uncertainty on the offline track and muon reconstruction efficiency is taken as 2% [33] and 2% [30] respectively. The uncertainty on the track momentum scale is taken as 1.5% [30].

The uncertainty on the luminosity is taken as 2.2% [34]. Table 1 summarizes the systematic uncertainties considered in this analysis. It also lists the range of the statistical uncertainty in the final selection for all the signal points. The bracketed values indicate the range of uncertainties measured over all the signal points. The total uncertainty on the signal acceptance is the combination of the individual contributions listed above and the statistical uncertainty in the final selection. The latter is included to account for the limited nature of the signal MC sample.

Table 1: Sources of systematic uncertainty and corresponding relative uncertainties. The total uncertainty on the signal acceptance is obtained by summing in quadrature the seven contributions and the statistical uncertainty in the final selection. The bracketed values give the range of the uncertainty for the different signal points.

Source of systematic uncertainty	Relative Uncertainty (%)
Signal efficiency	
Ionization energy loss scale	[0–1]
$1/\beta$ scale	[0–18]
Pile-up reweighting	[0–1]
Trigger efficiency	23
Track reconstruction efficiency	2
Muon reconstruction efficiency	2
Track momentum scale	1.5
Statistical uncertainty in the final selection	[1–11]
Total uncertainty on signal acceptance	[23–31]
Background prediction	20
Integrated luminosity	2.2

The uncertainty on the theoretical cross section due to the choice of PDF is estimated following the PDF4LHC recommendation [35], but not included into the final limits computation. The PDF uncertainties are less than 14% for all the signal points considered.

7 Results

For each signal model and mass point, the I_{as} and $1/\beta$ thresholds are varied to minimize the signal cross section value for which a discovery would be achieved, where discovery is defined as the expected mean significance of the observed excess being greater than 5 standard deviations with at least 5 observed candidates. Only thresholds with at least 25 events in the A, B, and C regions and no more than 1000 events in the D region are considered. The I_{as} and $1/\beta$ thresholds are varied in steps of 0.025.

The observed numbers of the candidate tracks are consistent with the expected background. Table 2 lists the relevant details for each signal point. We compute 95% CL exclusion limits on the observed cross section with a CLs approach where p-values are computed with a profile likelihood technique that uses a lognormal probability distribution function for the nuisance parameters. The latter are the integrated luminosity, the signal acceptance and the expected background in the signal region. The mass limits are obtained from the crossing point between theoretical predictions and observed cross section limits. We used a z-score statistic [36] to calculate the significance, which is a one sided probability of an upward background fluctuation, expressed in Gaussian sigmas. The observed cross section limits for multi-charged HSCPs with Q= 1e, 2e, 3e, 4e and 5e have been plotted as a function of their mass in Fig. 6. The observed cross section limits for multi-charged HSCPs with a fixed mass is plotted as a function of their electric charge in Fig. 7. Both Figs. 6 and 7 also show the theory cross section values for all the signal points considered. The green band surrounding the theory curves represent the uncertainty on the theory cross section values due to the choice of the PDF. Lower limits are computed on the masses of multi-charged HSCPs with Q= 1e, 2e, 3e, 4e and 5e of 427, 489, 545, 572 and 504 GeV/c^2, respectively. For multi-charged HSCPs with charge $\geq$ 1e, 95% CL limits on the charge for masses of 100, 200, 300, 400, 450, and 500 GeV/c^2 exclude charges 1–5e, 1–5e, 1–5e, 1–5e, 1.3–5e, and 2.2–5e, respectively. Figure 8 shows the ratio of the observed and expected cross section limits for all the signal points. The observed cross section limits lie within the 1σ band.

8 Conclusions

We have searched for slow moving and highly ionizing particles with the 2011 data recorded with the CMS detector. Ionization is measured with the silicon tracker and TOF with the muon system. Background is predicted with a data driven ABCD method. We observe no significant excess over prediction. We have set 95% CL upper limits on the Drell-Yan production cross sections of multi-charged HSCPs. The lower limits on the masses of stable, weakly-interacting particles with Q= 1e, 2e, 3e, 4e and 5e are 427, 489, 545, 572 and 504 GeV/c^2, respectively. For long-lived, weakly interacting particles with charge $\geq$ 1e, 95% CL limits on the charge for masses of 100, 200, 300, 400, 450, and 500 GeV/c^2 exclude charges 1–5e, 1–5e, 1–5e, 1–5e, 1.3–5e, and 2.2–5e, respectively.

References

[1] M. Fairbairn et al., "Stable massive particles at colliders", *Phys. Rept.* **438** (2007) 1–63, doi:10.1016/j.physrep.2006.10.002, arXiv:hep-ph/0611040.

[2] M. Drees and X. Tata, "Signals for heavy exotics at hadron colliders and supercolliders", *Phys. Lett.* **B252** (1990) 695–702, doi:10.1016/0370-2693(90)90508-4.

[3] D0 Collaboration, "Search for Long-Lived Charged Massive Particles with the D0 Detector", *Phys. Rev. Lett.* **102** (2009) 161802, doi:10.1103/PhysRevLett.102.161802, arXiv:0809.4472.

[4] CDF Collaboration, "Search for Long-Lived Massive Charged Particles in 1.96 TeV $\bar{p}p$ Collisions", *Phys. Rev. Lett.* **103** (2009) 021802, doi:10.1103/PhysRevLett.103.021802, arXiv:0902.1266.

[5] CMS Collaboration, "Search for Heavy Stable Charged Particles in pp collisions at $\sqrt{s} = 7$ TeV", *JHEP* **03** (2011) 024, doi:10.1007/JHEP03(2011)024, arXiv:1101.1645.

Table 2: Results of optimization for each signal point. The final selection along with the predicted and observed number of events are listed.

Mass (GeV/c^2)	I_{as} Cut	$1/\beta$ Cut	Prediction	Data
$Q = 1e$				
100	0.325	1.250	0.09 ± 0.02	0
200	0.300	1.275	0.09 ± 0.02	0
300	0.300	1.275	0.09 ± 0.02	0
350	0.325	1.250	0.09 ± 0.02	0
400	0.300	1.275	0.09 ± 0.02	0
450	0.300	1.275	0.09 ± 0.02	0
500	0.325	1.250	0.09 ± 0.02	0
$Q = 2e$				
100	0.350	1.200	0.22 ± 0.05	0
200	0.350	1.225	0.11 ± 0.03	0
300	0.350	1.225	0.11 ± 0.03	0
350	0.350	1.225	0.11 ± 0.03	0
400	0.350	1.225	0.11 ± 0.03	0
450	0.350	1.225	0.11 ± 0.03	0
500	0.350	1.225	0.11 ± 0.03	0
$Q = 3e$				
100	0.350	1.125	2.25 ± 0.55	3
200	0.350	1.225	0.11 ± 0.03	0
300	0.350	1.225	0.11 ± 0.03	0
350	0.350	1.225	0.11 ± 0.03	0
400	0.350	1.225	0.11 ± 0.03	0
450	0.350	1.225	0.11 ± 0.03	0
500	0.350	1.225	0.11 ± 0.03	0
550	0.350	1.225	0.11 ± 0.03	0
600	0.350	1.225	0.11 ± 0.03	0
$Q = 4e$				
100	0.350	1.100	4.96 ± 1.21	5
200	0.350	1.225	0.11 ± 0.03	0
300	0.350	1.225	0.11 ± 0.03	0
400	0.350	1.225	0.11 ± 0.03	0
450	0.350	1.225	0.11 ± 0.03	0
500	0.350	1.225	0.11 ± 0.03	0
550	0.350	1.225	0.11 ± 0.03	0
600	0.350	1.225	0.11 ± 0.03	0
$Q = 5e$				
100	0.350	1.075	10.40 ± 2.60	10
200	0.350	1.200	0.22 ± 0.05	0
300	0.350	1.200	0.22 ± 0.05	0
400	0.350	1.225	0.11 ± 0.03	0
450	0.350	1.225	0.11 ± 0.03	0
500	0.350	1.225	0.11 ± 0.03	0
550	0.350	1.225	0.11 ± 0.03	0

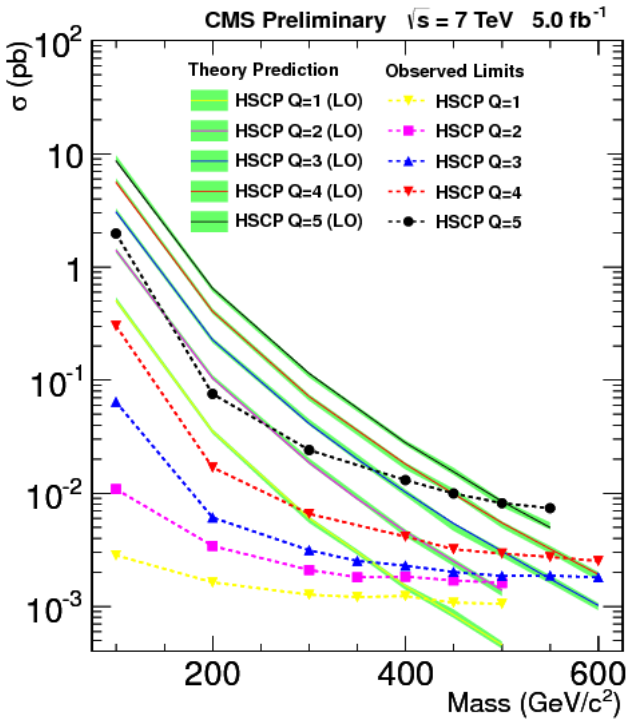

Figure 6: Theoretical cross sections and observed 95% CL cross section limits as a function of the multi-charged HSCP mass. The green bands represent the uncertainty on the theory cross section values due to the choice of the PDF.

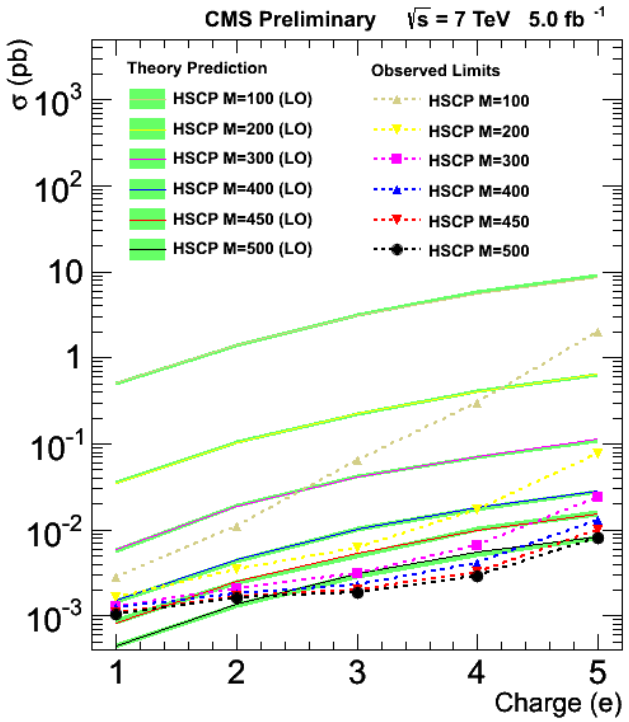

Figure 7: Theoretical cross sections and observed 95% CL cross section limits as a function of the multi-charged HSCP electric charge. The green bands represent the uncertainty on the theory cross section values due to the choice of the PDF.

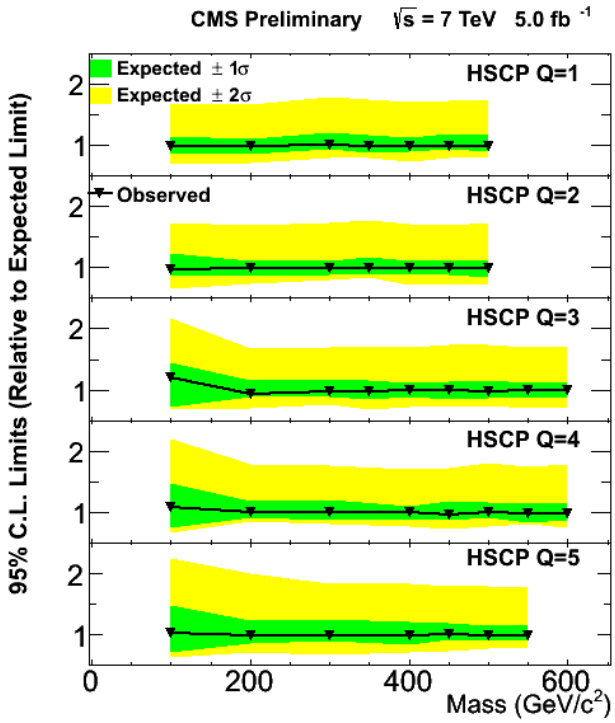

Figure 8: The ratio of the observed cross section limits to the expected cross section limits for Q=1e, 2e, 3e, 4e and 5e. The 1σ (green) and 2σ (yellow) bands are also shown.

[6] ATLAS Collaboration, "Search for stable hadronising squarks and gluinos with the ATLAS experiment at the LHC", *Phys. Lett.* **B701** (2011) 1–19, doi:10.1016/j.physletb.2011.05.010, arXiv:1103.1984.

[7] ATLAS Collaboration, "Search for Heavy Long-Lived Charged Particles with the ATLAS detector in pp collisions at $\sqrt{s} = 7$ TeV", *Phys. Lett.* **B703** (2011) 428–446, doi:10.1016/j.physletb.2011.08.042, arXiv:1106.4495.

[8] ATLAS Collaboration, "Search for Massive Long-lived Highly Ionising Particles with the ATLAS Detector at the LHC", *Phys. Lett.* **B698** (2011) 353–370, doi:10.1016/j.physletb.2011.03.033, arXiv:1102.0459.

[9] CMS Collaboration, "Search for Heavy Stable Charged Particles in pp collisions at $\sqrt{s} = 7$ TeV", *Phys. Lett.* **B713** (2012) 408–433, doi:10.1016/j.physletb.2012.06.023, arXiv:1205.0272.

[10] T. Adams, "Searches for Long-lived Particles at the Tevatron Collider", *Mod. Phys. Lett.* **A23** (2008) 371–385, doi:10.1142/S0217732308026467, arXiv:0802.1048.

[11] J. Chen and T. Adams, "Heavy stable charged particle searches at the LHC", *Int. J. Mod. Phys.* **A26** (2011) 3315–3335, doi:10.1142/S0217751X11053912.

[12] B. C. Allanach et al., "The Snowmass points and slopes: Benchmarks for SUSY searches", *Eur. Phys. J.* **C25** (2002) 113–123, doi:10.1007/s10052-002-0949-3, arXiv:hep-ph/0202233.

[13] G. R. Farrar and P. Fayet, "Phenomenology of the Production, Decay, and Detection of New Hadronic States Associated with Supersymmetry", *Phys. Lett.* **B76** (1978) 575.

[14] H. Baer, K.-m. Cheung, and J. F. Gunion, "A Heavy gluino as the lightest supersymmetric particle", *Phys. Rev.* **D59** (1999) 075002, doi:10.1103/PhysRevD.59.075002, arXiv:hep-ph/9806361.

[15] R. Barbieri, G. Marandella, and M. Papucci, "Breaking the electroweak symmetry and supersymmetry by a compact extra dimension", *Phys. Rev.* **D66** (2002) 095003, doi:10.1103/PhysRevD.66.095003, arXiv:hep-ph/0205280.

[16] A. Kusenko and M. E. Shaposhnikov, "Supersymmetric Q-balls as dark matter", *Phys. Lett.* **B418** (1998) 46–54, doi:10.1016/S0370-2693(97)01375-0, arXiv:hep-ph/9709492.

[17] B. Koch, M. Bleicher, and H. Stoecker, "Black holes at LHC?", *J. Phys.* **G34** (2007) S535–542, doi:10.1088/0954-3899/34/8/S44, arXiv:hep-ph/0702187.

[18] J. S. Schwinger, "Magnetic charge and quantum field theory", *Phys. Rev.* **144** (1966) 1087–1093, doi:10.1103/PhysRev.144.1087.

[19] D. Fargion, M. Khlopov, and C. A. Stephan, "Cold dark matter by heavy double charged leptons?", *Class. Quant. Grav.* **23** (2006) 7305–7354, doi:10.1088/0264-9381/23/24/008, arXiv:astro-ph/0511789.

[20] CMS Collaboration, "The CMS experiment at the CERN LHC", *JINST* **3** (2008) S08004, doi:10.1088/1748-0221/3/08/S08004.

[21] T. Sjöstrand, S. Mrenna, and P. Z. Skands, "PYTHIA 6.4 Physics and Manual", *JHEP* **05** (2006) 026, doi:10.1088/1126-6708/2006/05/026, arXiv:hep-ph/0603175.

[22] J. Alwall, M. H. F. Maltoni, O. Mattelaer et al., "MadGraph 5 : Going Beyond", *JHEP* **06** (2011) 128, doi:10.1007/JHEP06(2011)128, arXiv:1106.0522.

[23] N. Davidson, G. Nanava, T. Przedzinski et al., "Universal Interface of TAUOLA Technical and Physics Documentation", *Comput. Phys. Commun.* **183** (2012) 821–843, doi:10.1016/j.cpc.2011.12.009, arXiv:1002.0543.

[24] J. Pumplin et al., "New Generation of Parton Distributions with Uncertainties from Global QCD Analysis", *JHEP* **07** (2002) 012, doi:10.1088/1126-6708/2002/07/012, arXiv:hep-ph/0201195.

[25] R. Field, "Physics at the Tevatron", *Acta Phys. Polon.* **B39** (2008) 2611.

[26] R. Field, "Studying the underlying event at CDF and the LHC", arXiv:1003.4220.

[27] S. Agostinelli et al., "GEANT4-a simulation toolkit", *Nucl. Instrum. Meth. A* **506** (2003) 250, doi:10.1016/S0168-9002(03)01368-8.

[28] J. Allison et al., "Geant4 developments and applications", *IEEE Trans. Nucl. Sci.* **53** (2006) 270–278, doi:10.1109/TNS.2006.869826.

[29] Particle Data Group Collaboration, "Review of particle physics", *J. Phys.* **G37** (2010) 075021, doi:10.1088/0954-3899/37/7A/075021.

[30] CMS Collaboration, "Performance of muon reconstruction in pp collisions at $\sqrt{s} = 7$ TeV", *CMS Physics Analysis Summary* **CMS-PAS-MUO-10-004** (2010).

[31] CMS Collaboration, "Search for Heavy Stable Charged Particles in pp collisions at $\sqrt{s} = 7$ TeV", *CMS Physics Analysis Summary* **CMS-PAS-EXO-11-022** (2011).

[32] CMS Collaboration, "Single-Particle Response in the CMS Calorimeters", *CMS Physics Analysis Summary* **CMS-PAS-JME-10-008** (2010).

[33] CMS Collaboration, "Measurement of Tracking Efficiency", *CMS Physics Analysis Summary* **CMS-PAS-TRK-10-002** (2010).

[34] CMS Collaboration, "Absolute Calibration of the CMS Luminosity: Summer 2011 update", *CMS Physics Analysis Summary* **CMS-PAS-EWK-11-001** (2011).

[35] M. Botje, J. Butterworth, A. Cooper-Sarkar et al., "The PDF4LHC Working Group Interim Recommendations", arXiv:1101.0538.

[36] R. D. Cousins, J. T. Linnemann, and J. Tucker, "Evaluation of three methods for calculating statistical significance when incorporating a systematic uncertainty into a test of the background-only hypothesis for a Poisson process", *Nucl. Instrum. Meth.* **A595** (2008) 480–501, doi:10.1016/j.nima.2008.07.086.